

## Electrochemical and Photocatalytic Properties of Ru-doped TiO<sub>2</sub> Nanostructures for Degradation of Methyl Orange Dye

Baoshan Gong<sup>1,2</sup>, Pei Wu<sup>1,2,\*</sup>, Jia Yang<sup>1,2</sup>, Xuanwei Peng<sup>1,2</sup>, Hongwen Deng<sup>1,2</sup>, Gaohong Yin<sup>1,2</sup>

<sup>1</sup> School of Civil Engineering and Architecture, Chongqing University of Science and Technology, Chongqing 401331, China

<sup>2</sup> Chongqing Xin Yun Chuang Institute of Environmental Protection Research Co. Ltd, Chongqing 402566, China

\*E-mail: [wplw666@126.com](mailto:wplw666@126.com)

Received: 1 October 2020 / Accepted: 25 November 2020 / Published: 31 December 2020

---

This study was focused on chemical synthesis of the pure TiO<sub>2</sub> nanorods and Ru-doped TiO<sub>2</sub> nanorods and their applications as photocatalyst for photodegradation of the methyl orange (MO) dye under UV and visible irradiations. The morphology, crystallinity, optical, electrochemical and photocatalyst properties of prepared films were characterized by FESEM, XRD, UV-visible absorption, electrochemical impedance spectroscopy (EIS) and photodegradation analyses. The FESEM and XRD studies showed both of films were synthesized in nanorod shape and anatase crystal phase. The optical studies indicate that the optical band gap values were obtained 3.37 eV and 3.22 eV for nanostructured pure TiO<sub>2</sub> and Ru-doped TiO<sub>2</sub> films, respectively. EIS analysis indicates that Ru-doped TiO<sub>2</sub> film exhibited lower recombination rate of photo-excited carriers through effective separation of the photogenerated electron-hole pairs. Photodegradation studies of MO show that the degradation rate significantly was improved by Ru doping and the complete removal of MO were obtained after 55 and 45 minutes under UV and sunlight irradiation, respectively. While, degradation efficiency of MO on pure TiO<sub>2</sub> photocatalyst were achieved 57.0 % and 4.8 % after 60 minutes UV and sunlight irradiations, respectively. Therefore, the photodegradation rate of doped film was remarkably enhanced under both UV and sunlight irradiations. Moreover, photocatalytic activity was remarkably promoted under sunlight on doped photocatalyst because of narrowing optical band gaps.

---

**Keywords:** Photodegradation; Methyl orange dye; Ru-doped TiO<sub>2</sub>; Electrochemical impedance spectroscopy; Degradation efficiency

### 1. INTRODUCTION

TiO<sub>2</sub> as an attractive semiconductor material is extensively used in lithium-ion batteries, solar cells, photovoltaic devices, microelectronics and photocatalysts due to its simple manufacturing, cheap cost, great chemical and physical stability and nontoxicity. Among the applications, TiO<sub>2</sub>-based

photocatalysts have been shown excellent efficiency in environmental and energy area such as water treatment systems, electrochemical sensors, hydrogen evolution, air purifications and *air*-conditioning systems, self-cleaning/self-disinfecting surfaces, antibacterial tiles, CO<sub>2</sub> Conversion, hydrogen evolution and clean hydrogen energy generation [1, 2].

For many years, study and development of the TiO<sub>2</sub>-based photocatalyst devices have been the big challenge for researchers. These studies have been conducted through synthesis of the various TiO<sub>2</sub> nanostructures and TiO<sub>2</sub> based hybrid and composite systems due to enhancement of durability and chemical and mechanical stability of TiO<sub>2</sub>-based photocatalysts [3]. High effective surface area and high porosity of nanostructured electrodes increase the sensitivity and reactivity to UV and visible lights and improve the absorption ability of chemical species [4-7].

Furthermore, the doping process has been widely used for promoting the photocatalytic efficiency through enhancement of charge separation and electron transfer rate, and optical properties. For example, Zhang et al. [8] and Li et al. [9] prepared Mn-doped TiO<sub>2</sub> and Fe-doped TiO<sub>2</sub> photocatalysts, respectively and showed the band gap of the doped photocatalysts was narrowed because of introduction of dopant into TiO<sub>2</sub> matrix and generation of impurity levels near the of the conduction band of TiO<sub>2</sub>. Narrowing the band gap leads to red-shifting the photoexcitation activity of semiconductors. Therefore, the photochemical activity of doped TiO<sub>2</sub>-based photocatalysts not only observed in the UV region but also their photocatalytic performances are promoted in the visible light region and under sunlight irradiation.

It is the considerable point that doping process depended on technique, dopant concentration and dopant type shows negative and positive effects on optical and photocatalytic properties of nanostructured semiconductors [10-12]. On the other hand, the dopant can form defects as charge recombination centers in TiO<sub>2</sub> matrix and shows the negative effect on the separation of photoexcited carriers. Moreover, some defects can impede the formation of oxygen radicals in the photocatalysis mechanism [13, 14]. Therefore, the studies have been carried out for optimization of the photocatalysis performance by controlling the doped TiO<sub>2</sub> synthesis parameters. Accordingly, this study revealed the synthesis Ru-doped TiO<sub>2</sub> nanorods film and its application as a photocatalyst for degradation of MO.

## 2. EXPERIMENTAL

### 2.1 preparation of photocatalysts

In order to the preparation of photocatalysts, the transparent mixture solution was prepared from 25 minutes stirring of 1 M TiCl<sub>4</sub> (≥ 99.0 %, Sigma-Aldrich, UK), ethanol (99.0%, Shandong Baovi Energy Technology Co., Ltd., China) and triethanolamine (99.0 %, Hebei Ruiyao Biotechnology Co., Ltd., China) in volume ratio of 1:4:2. Then, to synthesize Ru-doped TiO<sub>2</sub> nanorods and pure TiO<sub>2</sub> nanorods, 1mM RuCl<sub>3</sub>·xH<sub>2</sub>O (≥ 99.0 %, Sigma-Aldrich, UK) and 1mM ammonium hydroxide (99.5 %, Famouschem Technology Co., Ltd., Shanghai, China) solutions was added to the transparent solution in volume ratio 1:1:4 and 0:1:4, respectively under magnetic stirring in pH 9. After then, the prepared mixtures were ultra-sonicated and centrifuged for 120 and 30 minutes, respectively.

The centrifuged mixture was dropped on fluorine-doped tin oxide (FTO, Guangzhou Lepond Glass Co., Ltd., China) and transferred to an oven under 75 °C for 12 hours.

## 2.2. Analyses and measurements

The morphology of prepared pure TiO<sub>2</sub> nanorods and Ru-doped TiO<sub>2</sub> nanorods films was studied by field-emission scanning electron microscopy (FESEM, DSM 982 Gemini; Carl. Zeiss SMT, Cambridge, UK). The crystal structures of prepared films were analyzed by X-ray diffraction (XRD, X'pert MPD, Philips, Eindhoven, the Netherlands) which was operating at 40 kV and 25 mA in wavelength of CuK $\alpha$  ( $\lambda=1.5418$  Å). The optical absorption spectra prepared samples were studied using a UV-VIS spectrophotometer (U-3900/3900H, Hitachi, Tokyo, Japan). EIS experiments were carried out in frequency range from 10 to 10<sup>6</sup> Hz at AC voltage of 5 mV amplitude using potentiostat equipment (CHI 660D, CH Instrument Company, Shanghai, China) in a standard three-electrode electrochemical cell which containing Ag/AgCl electrode, Pt wire and prepared films as reference, counter and working electrodes, respectively. The electrolyte of EIS measurement was in 0.1 M KCl (99%, Lianyungang Dongtai Food Ingredients Co., Ltd., China) containing 5mM [Fe(CN)<sub>6</sub>]<sup>3-/4-</sup> (99.5%, Changzhou Qi Di Chemical Co., Ltd., China) solution.

The photocatalytic studies of the prepared films were measured via the photocatalytic oxidation of MO under UV (15 W, UV bench lamp) and sunlight irradiations. To establish an adsorption–desorption equilibrium between the films and MO solution, prior to the photocatalytic experiments the prepared MO solution was stirred in darkness for 30 minutes. Photodegradation experiments were carried out in a photocatalytic chamber which contained a photocatalyst (prepared films) and the prepared aqueous MO solution (organic dye wastewater) is generated during the air purification and the production in the printing and dyeing plant. The degradation efficiency (%) of MO was analyzed through the recorded absorption intensity of UV-Vis spectrophotometer at 461 nm by following equation:

$$\text{Degradation efficiency} = \frac{I_0 - I_t}{I_0} \times 100 = \frac{C_0 - C_t}{C_0} \times 100 \quad (1)$$

Where,  $I_0$  is the initial absorption intensity of MO solution and  $I_t$  is absorption intensity of MO solution during irradiation.  $C_0$  is the initial concentration of MO solution and  $C_t$  is concentration of MO solution after irradiation.

## 3. RESULTS AND DISCUSSION

### 3.1 Structure characterization of photocatalysts

Figure 1a and 1b depict FESEM images of pure TiO<sub>2</sub> and Ru-doped TiO<sub>2</sub> nanorods, respectively. As observed, Ru-doped TiO<sub>2</sub> nanostructures were synthesized in nanorod shape with average diameter and length of 50 nm and 450 nm, respectively. Moreover, FESEM images are shown that Ru-doping controlled the growth of nanocrystals via the *template-free chemical route*.

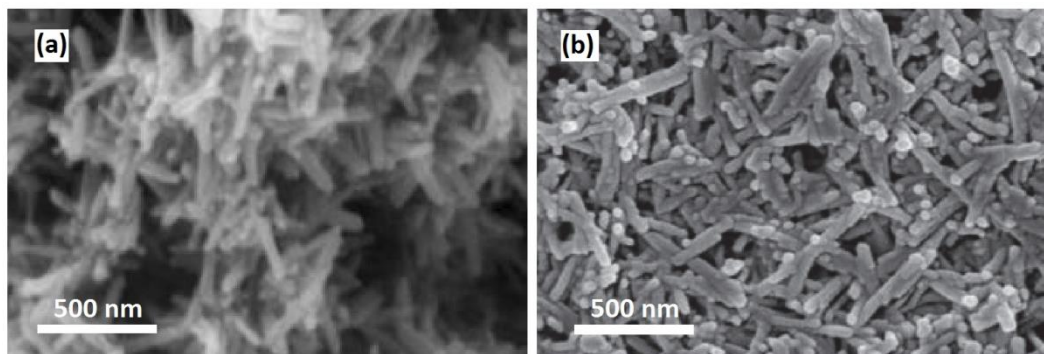


**Figure 1.** FESEM images of (a) pure TiO<sub>2</sub> and (b) Ru-doped TiO<sub>2</sub> nanorods.

The recorded XRD patterns of prepared films were displayed in Figure 2. As seen, all XRD patterns indicate the growth of nanorods in anatase crystal phase due to presents of diffraction peaks at  $2\theta = 25.08^\circ, 38.18^\circ, 47.98^\circ, 53.11^\circ, 54.96^\circ, 62.88^\circ, 68.86^\circ, 69.97^\circ,$  and  $75.11^\circ$  which associating to formation of the (101), (004), (200), (105), (211), (204), (116), (220), and (215) crystal planes (JCPDS card No. 21-127236), respectively. The Scherrer Equation was applied to calculate the average crystallite grain size ( $d$ ) as following formula [15]:

$$d = \frac{k\lambda}{\beta \cos \theta} \quad (2)$$

Where  $k$  is a dimensionless particle shape factor (0.9),  $\lambda$  is the wavelength of  $Cu-K\alpha$  (0.5406 nm),  $\beta$  is the line broadening at half the maximum intensity, and  $\theta$  is the Bragg angle of (101) plane. The crystallite grain size of pure TiO<sub>2</sub> and Ru-doped TiO<sub>2</sub> nanorods were obtained 17.83 and 17.88 nm, respectively which indicates the doping process did not make any remarkable change on the crystallite grain size in films. Furthermore, it was not recorded any new diffraction peak for formation Ru crystal phase after doping process which implying the Ru incorporation in anatase TiO<sub>2</sub> lattice as host that it is similar to reports of doping of Ru into the TiO<sub>2</sub> by Ismael [16] and Rajaramanan et al. [17].

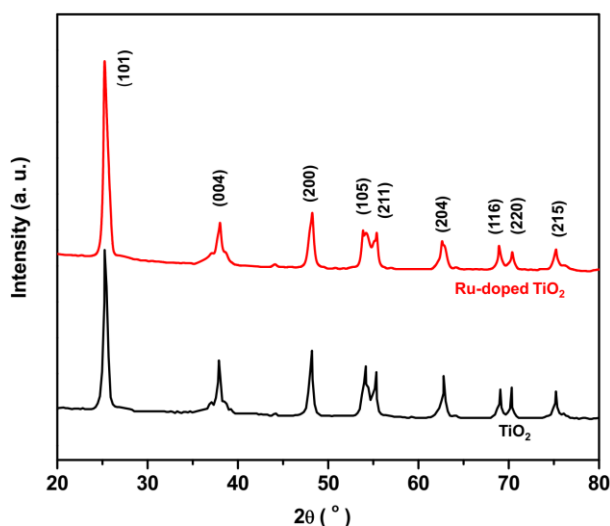


**Figure 2.** The recorded XRD patterns of (a) pure TiO<sub>2</sub> and (b) Ru-doped TiO<sub>2</sub> nanorods films.

### 3.2 Optical characterization of photocatalysts

The recorded absorption spectra of the pure TiO<sub>2</sub> and Ru-doped TiO<sub>2</sub> nanorods in room temperature are displayed in Figure 3a. The red shift of the absorption edge of Ru-doped TiO<sub>2</sub> film is observed toward pure TiO<sub>2</sub> film which could be related to narrowing the band gap energy due to the presence of Ru levels in the energy gap of TiO<sub>2</sub> [18, 19]. This shows the absorption range of pure TiO<sub>2</sub> limited to UV region and metal ion doping can enhance the photoactivation range of film to visible region [4]. Moreover, the absorption is increased after doping which attributing to metal higher absorption nature and formation of dipole active states in the band gap of the TiO<sub>2</sub> [20]. These redshift of absorption edge of nanostructured semiconductors by metal ion doping was also reported by Deng et al. [21] and El Mragui et al. [22]. To determination of film's optical band gap energy ( $E_g$ ), the Tauc equation was applied as the following formula [23, 24]:

$$(\alpha h\nu)^{\frac{1}{2}} = A(h\nu - E_g) \quad (3)$$

Where  $\alpha$  is absorption coefficient,  $h$  is Planck's constant ( $4.1357 \times 10^{-15}$  eV s), and  $\nu$  is the frequency of light. As seen in Figure 3b, the optical band gap values are obtained 3.37 eV and 3.22 eV for nanostructured pure TiO<sub>2</sub> and Ru-doped TiO<sub>2</sub> films, respectively. The narrowing of the band gap can be related to the formation of oxygen vacancies under the doping process which can enhance the defects energy level below the conduction band and shift its edge into the forbidden gap [25].

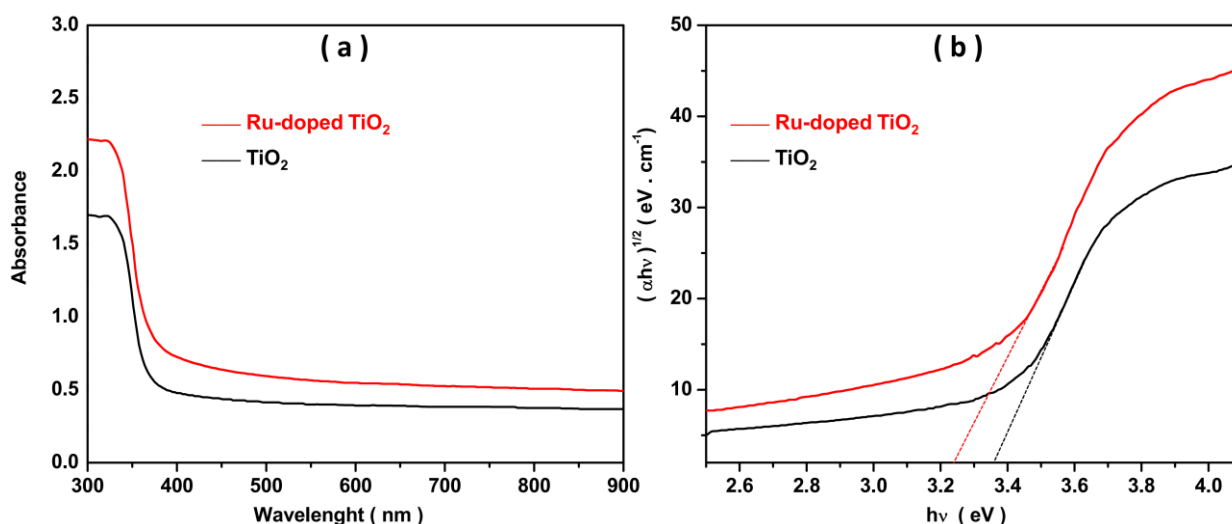


**Figure 3.** (a) The recorded absorption spectra and (b) the Tauc plots ( $(\alpha h\nu)^2$  vs photon energy) of the pure TiO<sub>2</sub> and Ru-doped TiO<sub>2</sub> nanorods in room temperature.

### 3.3 Electrochemical characterization of photocatalysts

In order to study the transfer and recombination of the charge at interfaces of films and electrolytes, the EIS measurements were recorded in 0.1 M KCl containing 5mM [Fe(CN)<sub>6</sub>]<sup>3-/4-</sup> redox probe solution with frequency range of 10 Hz to 10<sup>6</sup> Hz at AC voltage of 5 mV amplitude. Figure 4 shows the Nyquist plots of EIS analysis of the pure TiO<sub>2</sub> and Ru-doped TiO<sub>2</sub> electrodes. As observed,

the Ru-doped TiO<sub>2</sub> film shows the smaller semicircle than pure TiO<sub>2</sub> film which is associated with more interfacial charge transfer and lower recombination rate of photo-excited carriers through effective separation of the photogenerated electron-hole pairs [26, 27]. These observations can be related to the conduction band shift which can decrease energy loss and facilitates the photo-excited carriers [28].

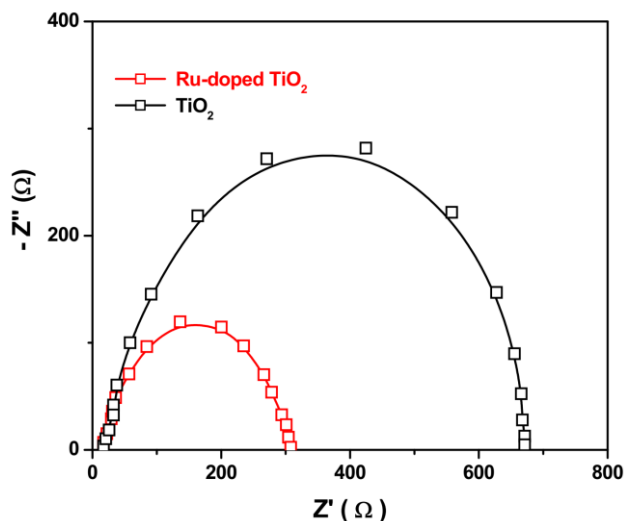


**Figure 4.** Nyquist plots of the pure TiO<sub>2</sub> and Ru-doped TiO<sub>2</sub> electrodes in 0.1 M KCl containing 5mM [Fe(CN)<sub>6</sub>]<sup>3-/4-</sup> redox probe solution with frequency range of 10 Hz to 10<sup>6</sup> Hz at AC voltage of 5 mV amplitude.

### 3.4 Photodegradation study of photocatalysts

Figures 5a and 5b show the photocatalytic degradation efficiency of MO in absent pure TiO<sub>2</sub> and Ru-doped TiO<sub>2</sub> photocatalysts under UV and sunlight irradiations, respectively. The higher degradation for Ru-doped TiO<sub>2</sub> efficiency is observed under both light irradiations and the complete removal of MO are obtained after 55 and 45 minutes under UV and sunlight irradiations, respectively. While, degradation efficiency of MO on pure TiO<sub>2</sub> photocatalyst is achieved 57.0 % and 4.8 % after 60 minutes UV and sunlight irradiations, respectively. The degradation rate significantly is improved by Ru doping. Figure 7 shows the comparison of photocatalyst performance after 20, 40 and 60 minutes irradiation of UV and sunlight which demonstrates the enhancement of photocatalytic activity under sunlight on doped photocatalyst because of narrowing optical band gap [29]. Therefore, the photocatalytic study of MO was performed on Ru-doped TiO<sub>2</sub> film under sunlight irradiation. Table 1 presents a comparison between the degradation performances of TiO<sub>2</sub>-based photocatalysts of this study and the other reported literature for degradation of MO. As seen, the prepared Ru-doped TiO<sub>2</sub> photocatalyst shows better or comparable photocatalytic performance for degradation 20 mg l<sup>-1</sup> of MO under both UV and visible irradiations. Therefore, the novelty of this study is the preparation of the TiO<sub>2</sub>-based photocatalyst that shows excellent photodegradation activity under both UV and visible irradiations.

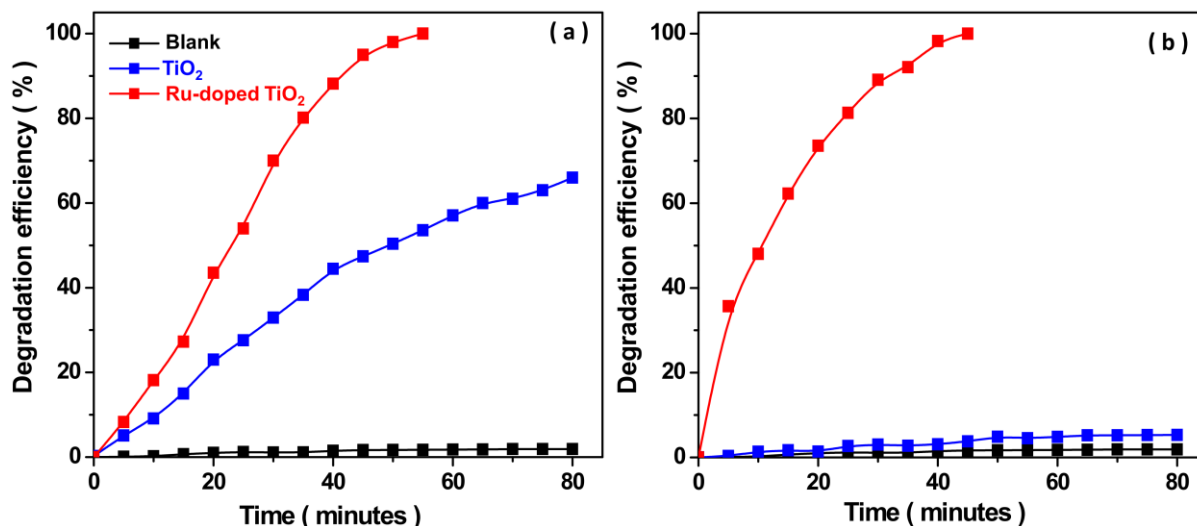


**Figure 5.** Photocatalytic degradation efficiency of MO on pure TiO<sub>2</sub> and Ru-doped TiO<sub>2</sub> electrodes under (a) UV and (b) sunlight irradiation.

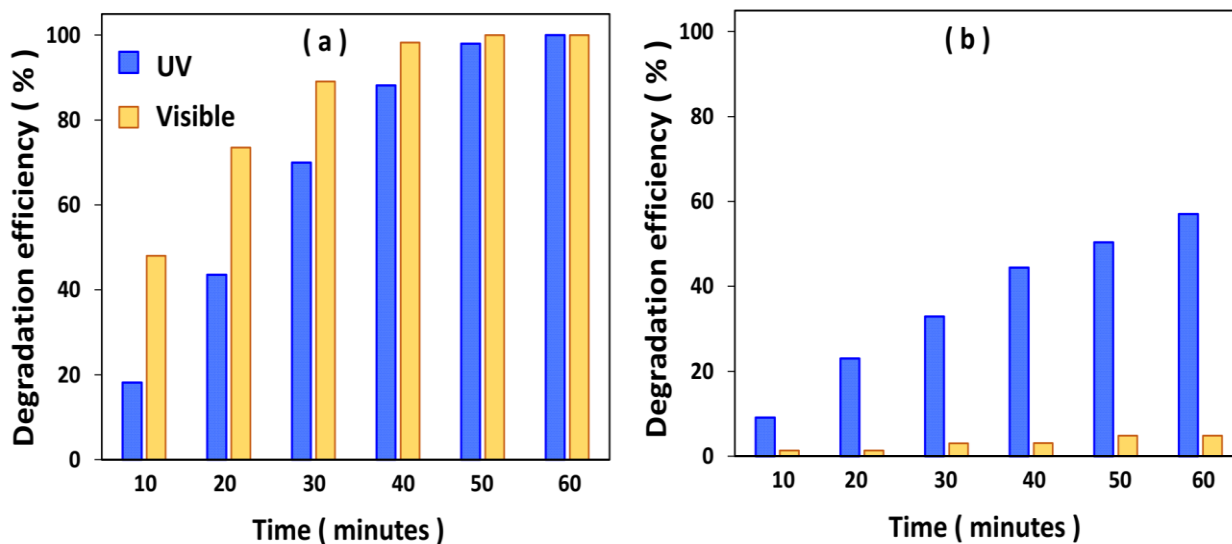


**Figure 6.** Photocatalytic degradation efficiency of MO on (a) pure TiO<sub>2</sub> and (b) Ru-doped TiO<sub>2</sub> electrodes after 20, 40 and 60 minutes irradiation of UV and sunlight.

**Table 1.** Comparison between the degradation performances of TiO<sub>2</sub> –based photocatalysts of this study and the other reported literature for degradation of MO.

Catalyst	MO concentration (mg l <sup>-1</sup> )	Light source	Degradation efficiency (%)	Irradiation time (minute)	ref
Fe <sub>2</sub> O <sub>3</sub> -TiO <sub>2</sub> composites	10	UV	87.8	25	[30]
Core-shell TiO <sub>2</sub> @α-Fe <sub>2</sub> O <sub>3</sub>	10	visible	96.6	16	[31]
Cu-doped TiO <sub>2</sub> nanoparticles	10	visible	98.0	45	[32]

Fe <sup>3+</sup> -doped TiO <sub>2</sub>	20	visible	70.0	360	[33]
Pt modified TiO <sub>2</sub>	20	UV	98.0	90	[34]
N-doped TiO <sub>2</sub> nanoparticles	20	visible	14.0	60	[35]
N-doped TiO <sub>2</sub>	20	UV	98.0	100	[36]
Fe-doped TiO <sub>2</sub> nanotubes	20	UV-visible	99.7	180	[37]
fluorinated mesoporous TiO <sub>2</sub> microspheres	20	UV	96.0	42	[38]
pure TiO <sub>2</sub> nanorods	20	UV	57.0	60	This work
pure TiO <sub>2</sub> nanorods	20	visible	5.0	60	This work
Ru-doped TiO <sub>2</sub> nanorods	20	UV	100	55	This work
Ru-doped TiO <sub>2</sub> nanorods	20	visible	100	45	This work

To study the repeatability, stability and recycling performance of Ru-doped TiO<sub>2</sub>, the MO degradation were measured over four recycles. Figure 7 shows that photocatalytic degradation of recycled samples was not seriously decreased (98.22 % to 97.51 %) which indicates the great stability for MO degradation over four recycles. The slight decrease in degradation efficiency mainly is related to the reduction of adsorption sites on the photocatalyst surface.

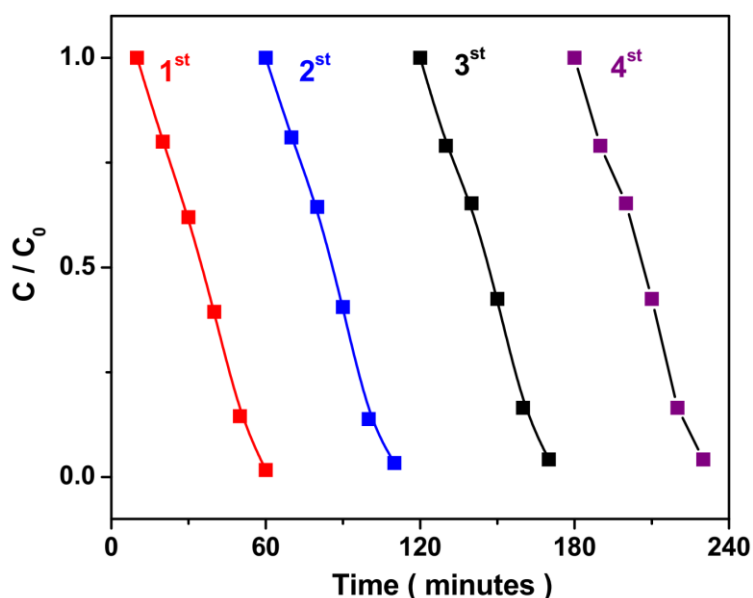
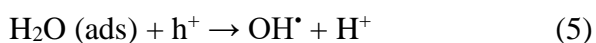
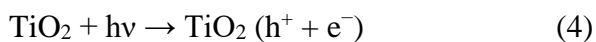


**Figure 7.** Recycling performance of Ru-doped TiO<sub>2</sub> for MO degradation under sunlight irradiations.

The main mechanism for photocatalytic degradation on TiO<sub>2</sub> surface is described as reactions (4) to (7) which contain the photogeneration of electron-hole pair and formation of other photo-induced active species such as hydroxyl radical (OH<sup>•</sup>) and superoxide radical anions (O<sub>2</sub><sup>•-</sup>) [39]:



The dye molecules are adsorbed on the nanostructured photocatalyst surface because of its high porous and high effective surface area. After irradiation the light, TiO<sub>2</sub> is photoexcited (reaction (4)) and photogenerated electrons can be transited from the valence band to the conduction band and photogenerated holes are left on the valence band. The incorporated Ru particles in TiO<sub>2</sub> lattice lead to easy photoactivation in the visible region that the photogenerated electrons can be injected to the conduction band of TiO<sub>2</sub> [40]. In the degradation process, the photo-induced active species attack and oxidize the organic pollutant. To determine the dominant photo-induced active species responsible for degradation of MO upon sunlight illumination, four quenching agents were separately added to four prepared MO solutions before the photodegradation measurements. These quenching agents include 0.1 mM solution of p-benzoquinone (BQ), tert-butyl alcohol (TBA), ammonium oxalate (AO) and AgNO<sub>3</sub> as quenching agents of O<sub>2</sub><sup>•-</sup>, OH<sup>•</sup>, h<sup>+</sup> and e<sup>-</sup> [41, 42], respectively. Figure 8 shows the degradation efficiency of MO is decreased in addition to all of quenching agents due to the trapping of the active species. As observed, degradation efficiency of MO exhibits impressively decrease in addition of TBA which specifying that OH<sup>•</sup> is the main reactive species in the photo-degradation of MO. This result is similar to reports of Shan et al. [40] for degradation of MO on Ag/TiO<sub>2</sub>/biochar composite surface.

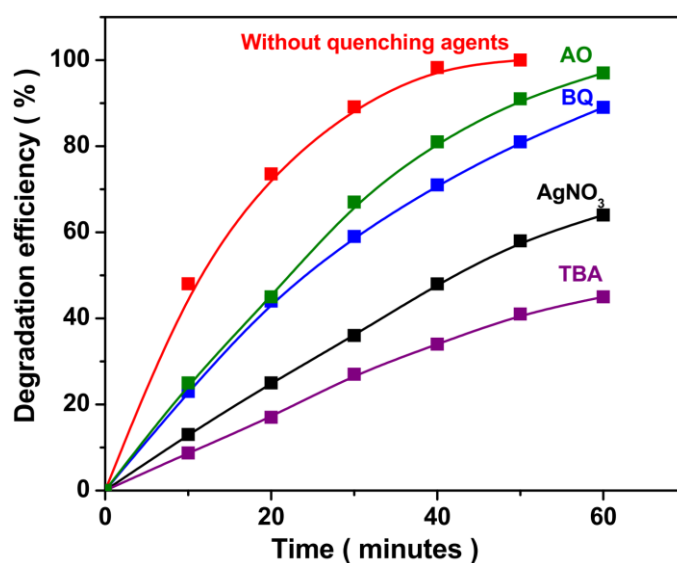


**Figure 8.** Photocatalytic degradation efficiency of MO on Ru-doped TiO<sub>2</sub> photocatalyst after addition of quenching agents and 60 minutes irradiation of sunlight.

#### 4. CONCLUSION

This study was carried out for preparation of the pure TiO<sub>2</sub> nanorods and Ru-doped TiO<sub>2</sub> nanorods films and their applications as photocatalyst for photodegradation of the MO under UV and visible irradiations. The pure and doped TiO<sub>2</sub> nanorods films were synthesized through the chemical method and their morphology, crystal structure, optical, electrochemical and photocatalyst properties were analyzed by FESEM, XRD, UV-visible absorption, EIS and photodegradation techniques, respectively. The FESEM and XRD results showed TiO<sub>2</sub> and Ru-doped TiO<sub>2</sub> nanostructures were synthesized in nanorod shape and anatase crystal phase. The optical studies show the redshift of the absorption edge of Ru-doped TiO<sub>2</sub> film was observed toward to pure TiO<sub>2</sub> film, which could related to narrowing the band gap energy due to the presence of Ru levels in the energy gap of TiO<sub>2</sub> and the formation the oxygen vacancies under doping process. The optical band gap values were obtained 3.37 eV and 3.22 eV for nanostructured pure TiO<sub>2</sub> and Ru-doped TiO<sub>2</sub> films, respectively. EIS studies showed that Ru-doped TiO<sub>2</sub> film exhibited lower recombination rate of photo-excited carriers through effective separation of the photogenerated electron-hole pairs. Photodegradation studies of MO showed that the degradation rate significantly was improved by Ru doping and the complete removal of MO were obtained after 55 and 45 minutes under UV and sunlight irradiations, respectively. While, degradation efficiency of MO on pure TiO<sub>2</sub> photocatalyst was achieved 57.0 % and 4.8 % after 60 minutes UV and sunlight irradiations, respectively. Moreover, photocatalytic activity was remarkably enhanced under sunlight on doped photocatalyst because of narrowing optical band gaps. Results indicated that OH<sup>•</sup> was the main reactive species in the photo-degradation of MO.

#### ACKNOWLEDGEMENT

The authors are grateful for the financial support provided by the project of Research on high efficiency fresh air purification technology (No. cstc2019jscx-msxmX0206).

#### References

1. K. Nakata and A. Fujishima, *Journal of photochemistry and photobiology C: Photochemistry Reviews*, 13 (2012) 169.
2. J. Rouhi, C.R. Ooi, S. Mahmud and M.R. Mahmood, *Materials Letters*, 147 (2015) 34.
3. R. Verma, J. Gangwar and A.K. Srivastava, *RSC advances*, 7 (2017) 44199.
4. S.A. Bakar and C. Ribeiro, *Journal of Photochemistry and Photobiology C: Photochemistry Reviews*, 27 (2016) 1.
5. Z. Savari, S. Soltanian, A. Noorbakhsh, A. Salimi, M. Najafi and P. Servati, *Sensors and Actuators B: Chemical*, 176 (2013) 335.
6. H. Savaloni, R. Savari and S. Abbasi, *Current Applied Physics*, 18 (2018) 869.
7. R. Dalvand, S. Mahmud, J. Rouhi and C.R. Ooi, *Materials Letters*, 146 (2015) 65.
8. K.-j. Zhang, X. Wei, X.-j. Li, S.-j. Zheng, X. Gang and J.-h. Wang, *Transactions of Nonferrous Metals Society of China*, 16 (2006) 1069.
9. Z. Li, W. Shen, W. He and X. Zu, *Journal of Hazardous Materials*, 155 (2008) 590.

10. R. Hassanzadeh, A. Siabi-Garjan, H. Savaloni and R. Savari, *Materials Research Express*, 6 (2019) 106429.
11. R.S. Dubey and S. Singh, *Results in Physics*, 7 (2017) 1283.
12. J. Rouhi, S. Mahmud, S.D. Hutagalung and S. Kakooei, *Journal of Micro/Nanolithography, MEMS, and MOEMS*, 10 (2011) 043002.
13. A. Kubacka, G. Colón and M. Fernández-García, *Catalysis Today*, 143 (2009) 286.
14. J. Rouhi, C.R. Ooi, S. Mahmud and M.R. Mahmood, *Electronic Materials Letters*, 11 (2015) 957.
15. H. Savaloni and R. Savari, *Materials Chemistry and Physics*, 214 (2018) 402.
16. M. Ismael, *New Journal of Chemistry*, 43 (2019) 9596.
17. T. Rajaramanan, M. Natarajan, P. Ravirajan, M. Senthilnathan and D. Velauthapillai, *Energies*, 13 (2020) 1532.
18. M.N. Islam and J. Podder, *Materials Science in Semiconductor Processing*, 121 (2021) 105419.
19. R. Mohamed, J. Rouhi, M.F. Malek and A.S. Ismail, *International Journal of Electrochemical Science*, 11 (2016) 2197.
20. R. Zhang, J. Zhao, Y. Yang, Z. Lu and W. Shi, *Computational Condensed Matter*, 6 (2016) 5.
21. Q. Deng, X. Han, Y. Gao and G. Shao, *Journal of Applied Physics*, 112 (2012) 013523.
22. A. El Mragui, Y. Logvina, L. Pinto da Silva, O. Zegaoui and J.C. Esteves da Silva, *Materials*, 12 (2019) 3874.
23. V. Mututu, A. Sunitha, R. Thomas, M. Pandey and B. Manoj, *International Journal of Electrochemical Science*, 14 (2019) 3752.
24. T. Malevu and R. Ocaya, *International Journal of Electrochemical Science*, 10 (2015) 4097.
25. S. Munir, S.M. Shah and H. Hussain, *Materials & Design*, 92 (2016) 64.
26. X. Gao, X. Liu, Z. Zhu, X. Wang and Z. Xie, *Scientific reports*, 6 (2016) 30543.
27. J. Rouhi, S. Kakooei, S.M. Sadeghzadeh, O. Rouhi and R. Karimzadeh, *Journal of Solid State Electrochemistry*, 24 (2020) 1599.
28. S. Wang, B. Liu, Y. Zhu, Z. Ma, B. Liu, X. Miao, R. Ma and C. Wang, *Solar Energy*, 169 (2018) 335.
29. W. Xie, R. Li and Q. Xu, *Scientific reports*, 8 (2018) 1.
30. L. Wu, H. Yan, J. Xiao, X. Li, X. Wang and T. Zhao, *Ceramics International*, 43 (2017) 14334.
31. Z. Lin, P. Liu, J. Yan and G. Yang, *Journal of Materials Chemistry A*, 3 (2015) 14853.
32. M. Hamadani, A. Reisi-Vanani and A. Majedi, *Applied Surface Science*, 256 (2010) 1837.
33. T. Tong, J. Zhang, B. Tian, F. Chen and D. He, *Journal of Hazardous Materials*, 155 (2008) 572.
34. M. Huang, C. Xu, Z. Wu, Y. Huang, J. Lin and J. Wu, *Dyes and pigments*, 77 (2008) 327.
35. S. Hu, A. Wang, X. Li and H. Löwe, *Journal of Physics and Chemistry of Solids*, 71 (2010) 156.
36. F. Peng, L. Cai, L. Huang, H. Yu and H. Wang, *Journal of Physics and Chemistry of Solids*, 69 (2008) 1657.
37. L. Deng, S. Wang, D. Liu, B. Zhu, W. Huang, S. Wu and S. Zhang, *Catalysis Letters*, 129 (2009) 513.
38. C. Yu, C.Y. Jimmy and M. Chan, *Journal of Solid State Chemistry*, 182 (2009) 1061.
39. D.D. Dionysiou, M.T. Suidan, E. Bekou, I. Baudin and J.-M. Laine, *Applied Catalysis B: Environmental*, 26 (2000) 153.
40. R. Shan, L. Lu, J. Gu, Y. Zhang, H. Yuan, Y. Chen and B. Luo, *Materials Science in Semiconductor Processing*, 114 (2020) 105088.
41. S. Tang, Z. Wang, D. Yuan, Y. Zhang, J. Qi, Y. Rao, G. Lu, B. Li, K. Wang and K. Yin, *International Journal of Electrochemical Science*, 15 (2020) 2470.

42. Q. Li, K. Wang, X. Lu, R. Luo, M. Zhang, C. Cui and G. Zhu, *International Journal of Electrochemical Science*, 15 (2020) 9256.

© 2021 The Authors. Published by ESG ([www.electrochemsci.org](http://www.electrochemsci.org)). This article is an open access article distributed under the terms and conditions of the Creative Commons Attribution license (<http://creativecommons.org/licenses/by/4.0/>).